1979, Proc. 20th U. S. Symposium Rock Mechanics, Austin, Texas, p. 35-49.
CONF-790606--10

STRENGTH AND DUCTILITY OF FOUR DRY IGNEOUS ROCKS AT LOW PRESSURES AND TEMPERATURES TO PARTIAL MELTING

CONF-790606--10

DE86 006476

by M. Friedman, J. Handin, N.G. Higgs, and J.R. Lantz,
Texas A & M Univ.

AS05-79ER10361

MASTER

This paper was presented at the 20th U.S. Symposium on Rock Mechanics, held in Austin, Texas, June 4-6, 1979. The material is subject to correction by the author. Permission to copy is restricted to an abstract of not more than 300 words. Write: Dr. Ken Gray, U. of Texas at Austin, Petroleum Engineering Dept.

ABSTRACT

Energy extraction from magma requires stable boreholes at relatively shallow depths (< 10 km) in rocks at temperatures of the order of 1000°C. Accordingly, the failure strengths, strains at failure, and associated deformation mechanisms of room-dry andesite, basalt, granodiorite, and obsidian are determined at temperatures to partial melting (> 1050°C), at confining pressures of 0 and 50 MPa, and a strain rate of 10^{-4}/s. The strength reductions of the crystalline rocks are more or less linear until they steepen suddenly with approach to melting. When that occurs, strengths vanish and deformations become quasiviscous. The obsidian is stronger than the crystalline rocks to 600°C where glass softening begins and strength goes to zero at 800°C. All rocks are brittle throughout the entire temperature range until melting or softening occurs. Shortenings at failure are 3 percent or less. The crystalline rocks tend to deform primarily by precursive microscopic extension fracturing and its coalescence into macroscopic faults. The abundance of load-induced fractures remains about constant, but thermal cracking increases with increasing temperature. Results from tests at 25°C on specimens that previously had been heated to 900-1000°C clearly show that the weakening of unconfined specimens is due to the thermal cracking. Weakening of confined specimens, however, probably is due to an inherent temperature effect on the load-induced fracturing process. Comparisons of instantaneous failure-strengths with stresses likely to occur at the walls of boreholes show that a hole as deep as 10 km in impermeable crystalline rock is not likely to fail under short-time loading even at 1000°C, unless the maximum in-situ horizontal stress is ≥ vertical stress and the hole is open (i.e., borehole pressure is zero).

INTRODUCTION

Borehole stability is one of many severe engineering problems to be anticipated should attempts ever be made to recover directly the geothermal energy stored in magma chambers, as temperatures of the order of 1000°C are expectable. How strong are the rocks to be drilled in this hostile environment? Previous laboratory work is not very helpful because virtually all testing above 500°C has been done at either atmospheric pressure[1] or very high confining pressures of 400 MPa or more[2,3,4]. What is needed is testing at high temperature but low confining pressure. Thus, under laboratory conditions that simulate the expectable natural environment of engineering concern, we are testing rock types that are likely candidates for drilling. Reported herein are the short-time ultimate strengths and ductilities of four room-dry igneous rocks--andesite, basalt, granodiorite, and obsidian--deformed at 0 and 50-MPa confining pressure, 25° to 1050°C, and a strain rate of 10^{-4}/s (unless otherwise noted). These strengths are then compared with the stresses developed at the wall of a borehole in an elastic medium at the appropriate temperatures and mean pressures.

References and illustrations at end of paper.

APPARATUS AND PROCEDURES

Some of the triaxial compression tests have been done in a screw-driven machine, similar to that designed by Heard[5], at strain rates of 10^{-4} and 10^{-7}/s on 0.9 by 2.0-cm specimens. Others, including all at temperatures above 400°C, have been carried out in the new apparatus briefly described below.

Cylindrical specimens, 2 cm in diameter and 4 cm in length, are axially loaded in a simple four-pole hydraulic press, driven by a variable-speed, constant-displacement, duplex oil pump so as to shorten specimens at constant axial strain rates of 10^{-4} or 10^{-6}/s. Force (up to 1 MN) is measured by a Baldwin CXX load-cell hooked to an X-Y recorder. Displacement is measured by a DCDT hooked to the same recorder.

The confining pressure of argon up to 300 MPa is generated by an intensifier driven by an air pump and charged by an oil-gas separater driven by a second air pump. It is measured by a precision Heise gauge and regulated by a Brown strip-chart recorder.

The triaxial cell, similar in design to that of Goetze[6], with an inside diameter of 3.8 cm and an

DISTRIBUTION OF THIS DOCUMENT IS UNLIMITED

DISCLAIMER

This report was prepared as an account of work sponsored by an agency of the United States Government. Neither the United States Government nor any agency Thereof, nor any of their employees, makes any warranty, express or implied, or assumes any legal liability or responsibility for the accuracy, completeness, or usefulness of any information, apparatus, product, or process disclosed, or represents that its use would not infringe privately owned rights. Reference herein to any specific commercial product, process, or service by trade name, trademark, manufacturer, or otherwise does not necessarily constitute or imply its endorsement, recommendation, or favoring by the United States Government or any agency thereof. The views and opinions of authors expressed herein do not necessarily state or reflect those of the United States Government or any agency thereof.

DISCLAIMER

Portions of this document may be illegible in electronic image products. Images are produced from the best available original document.

outside diameter of 16.5 cm, is made of 4340 steel, drawn to a hardness of Rockwell 34C for optimum toughness. Inside the cell the specimen is jacketed in a thin-walled copper sleeve and surrounded by the internal furnace. This furnace consists of two independently powered coils of Kanthal wire separated by a distance equal to the length of the specimen, and embedded in Norton EA 162 alumina and Sauereisen No. 78 electric-resistor cement prior to wrapping with Fiberfrax, refractory, insulating paper to the maximum diameter. The absence of furnace windings in the central region serves to flatten previously convex temperature profiles, related to the low conductivity of the sample. By adjusting the power distribution between the upper and lower windings, severe thermal gradients caused by convection in the gap between the furnace and the specimen assembly are subdued. For unconfined tests, nearly flat temperature profiles are achieved by dissipating only 40% of the total power to the upper furnace coil. For confined tests, convection in the dense argon confining-medium has been a bigger problem, but this has been overcome by infilling the annulus between the furnace wall and specimen with boron-nitride powder, an inert, non-abrasive material, combining excellent dielectric characteristics with good thermal conductivity, and effectively eliminating convection. Temperature is measured on the specimen by a thermocouple inserted through a hole in the lower plug and regulated by a West stepless controller. Furnace power is fed through Bridgman-type, insulated cones. Temperature differences along the length of the specimen are held to as small as 30°C at 1000°C, and temperature measurements are accurate to $\pm$ 5°C.

The cell is cooled externally by a water jacket, and loss of heat through the upper loading piston and lower plug is reduced by lucalox spacers, which are excellent thermal insulators, but which also have adequate compressive strengths at the temperatures of interest. Seals on the moving piston and lower closure can then be made by ordinary rubber O-rings.

Each test is done at a constant confining pressure of 0 or 50 MPa, a temperature between 25° and 1050°C, and a strain rate of 10^{-4}/s. True stress-strain curves are derived from the force-displacement record. Axial differential stress at each increment of axial strain is calculated from a corrected area assuming Poisson's ratio 0.25, volume conservation and homogeneous deformation assumed. Conventional strain is calculated by dividing the change in length by the original length, the displacement record having been corrected for elastic distortion of the apparatus, and expressed as percent shortening. The accuracies of stress, strain, and confining pressure are 2 to 3 percent.

"Undrained" tests are accomplished by placing a solid glass-hard steel or carbide spacer between the specimen and the lower lucalox spacer; whereas, for "drained" tests this spacer is hollow so that any fluids within the specimen can flow out through the thermocouple port in the lower plug and hence are at essentially atmospheric pressure.

In the triaxial compression test, the principal stresses are $\sigma_1 > \sigma_2 = \sigma_3 = p_c$ where p_c is effective confining pressure and compressive stresses are counted positive. Later on , we shall use the laboratory data to predict failure of the borehole where $\sigma_1 > \sigma_2 > \sigma_3$, and we shall assume that ultimate compressive strength, $(\sigma_1-\sigma_3)$, at failure is a function only of mean stress, $\sigma_m = (\sigma_1 + \sigma_2 + \sigma_3)/3$, and temperature. Thus for each test we compute $(\sigma_1-\sigma_3)$ and σ_m and list them together with the total shortening at macroscopic failure that serves as a measure of ductility (Tables 1-4).

Also listed is the angle θ between the load axis (σ_1) and the macroscopic fault, as measured with a contact goniometer outside the copper jacket. "Shattered" specimens have failed by multiple faulting, and θ cannot be determined.

STARTING MATERIALS

Mount Hood Andesite

Our sample was collected from a Recent flow, located just below the parking lot of Timberline Lodge on the south slope of Mount Hood. The block is pink and porphyritic with an aphanitic groundmass. Porosity varies from 10 to 12%. Phenocrysts comprise about 40% of the rock, 30% being plagioclase, 5% pyroxene, and about 1% each of hornblende, olivine, and magnetite. The feldspars are zoned, twinned labradorite, and along with the other phenocrysts, are conspicuously fractured. The long axes of the phenocrysts range up to 5 mm; overall they are randomly oriented, although in small domains they often show parallel alignment. Microfractures are confined to the phenocrysts, and none was observed to transect both phenocrysts and groundmass. The microfractures are randomly oriented, and the average number of microfractures per mm is less than 1 in the groundmass and about 7 in the phenocrysts.

The groundmass consists of small crystals (<1 mm) of lath-shaped feldspar, dispersed magnetite, and a small amount of interstitial glass. It completely envelopes the phenocrysts. This nearly holocrystalline groundmass should serve as the load-bearing framework that controls the gross mechanical behavior of the rock. A chemical analysis is given by Murase and McBirney[7] who also list liquidus temperatures of 1100°C for pyroxene, 1240°C for plagioclase, and 1210°C for the opaque oxides.

Charcoal Granodiorite

This rock is properly known as the St. Cloud Gray Granodiorite of Precambrian age from St. Cloud Minnesota; "Charcoal" is its trade name. Our sample was purchased from the Cold Springs Granite Co. in Minnesota. It is one of the rocks adopted as standard by the U.S. Bureau of Mines[8]. Its modal composition is: 38% labradorite, 25% orthoclase, 21% quartz, 12% hornblende and 5% biotite. Grain size ranges from < 0.1 to 10.0 mm and averages about 2 mm. Quartz crystals are free of deformation lamellae; but 49% exhibit undulose extinction, 43% are polygonized, and 12% are undeformed. Some 67% contain healed fractures, and 21% contain fresh fractures. The feldspars are all twinned and nearly all contain some fractures. Overall, however, the average number of microfractures per mm is less than 1.

There is a fracture anisotropy in this rock. Experimentally induced tensile fractures are controlled by pre-existing arrays of microfractures; ultrasonic velocity is minimum, and attenuation is maximum perpendicular to the plane of fracture anisotropy[9]. All

our test specimens are loaded perpendicular to this plane. Porosity is less than 0.1%.

Cuerbio Basalt

A large block of the Cuerbio Basalt of Early Pleistocene age was collected from the lower of two flows exposed in a roadcut along U.S. Highway 85, near the top of La Bajada Hill, south of La Cienega, New Mexico. The specimen contains some macroscopic, elongated vesicles up to 2 cm long. Sawed slabs from the block were X-rayed at Sandia Laboratories by Dr. E. J. Graeber and his associate, so that we could core our specimens from domains free of the larger vesicles. This approach worked successfully, and the few small vesicles (< 1.0 mm) exposed at the surface of some cylinders were filled with a high-temperature cement to prevent jacket failure. The reproducibility and consistent trends of the experimental data attest to the success of this approach. Porosity of test specimens ranges between 5 and 8%.

The basalt is dark gray and it contains an aphanitic groundmass, phenocrysts, and vesicles, both with maximum lengths of about 1 mm. Thin-section analyses reveal that the larger phenocrysts are composed of 80% euhedral, fractured olivine, 17% cleaved pyroxene, and 4% twinned and fractured feldspar; in aggregate these phenocrysts compose 14% of the rock. The groundmass (85%) is holocrystalline and consists of microphenocrysts of olivine and pyroxene (< 0.1 mm), magnetite (< 0.06 mm), and lath-shaped feldspars (up to 0.35 mm). These comprise 10%, 10%, and 80% of the groundmass, respectively. Microscopically, the rock shows a flow layering manifest by the dimensional alignment of feldspar laths in the groundmass and the larger olivine phenocrysts. All our specimens are loaded parallel to this planar anisotropy.

Newberry Rhyolite Obsidian

Our sample was collected from the north end of the Big Obsidian Flow along the trail southeast of Pauline Lake, Newberry Caldera, Oregon. The block contains flow banding which locally produces a planar anisotropy and complicates the coring of perfect, right-circular cylinders for experiments. Microscopically, this rock consists entirely of a clear, black glass which completely envelopes minute crystals of feldspar. The crystallites are strongly oriented dimensionally and reflect local, primary flow of lava prior to freezing. This fabric cannot be related to the experimental deformation; accordingly, petrofabric studies are macroscopic. A specimen deforms by either brittle fracture or by uniform flow with no macroscopic manifestation except barrelling. Data on chemical composition, viscosity, and other physical properties are given by Murase and McBirney[7].

EXPERIMENTAL RESULTS

Crystalline Rocks

Data sets for the instantaneous failure strength and strain of room-dry Mt. Hood Andesite, Charcoal Granodiorite, and Cuerbio Basalt, shortened at confining pressures of 0 and 50 MPa, temperatures to 1000°C, and a strain rate of 10^{-4}/s, are given in Tables 1, 2, and 3, and corresponding stress-strain curves appear in Figure 1. These data reveal the following significant facts.

(1) The reproducibility of data on strength and shortening at failure is reasonably good for specimens deformed under similar conditions and for specimens of different size deformed under the same conditions, but in a different apparatus (e.g., Table 2, specimens T1 and M3).

(2) The failure strengths of all three rocks decrease with increasing temperature at constant confining pressure and increase with increasing confining pressure at constant temperature (Fig. 2, 3, 4). The average strength-reduction of the andesite is essentially linear from 125 MPa at 25°C to 80 MPa at 1000° unconfined, and from 280 MPa at 25° to 195 MPa at 900°C, at 50-MPa confining pressure, or 1.2 and 2.4 MPa/25°C. Strength reductions for the granodiorite are much steeper. At 50 MPa, the reduction is slightly curvilinear from 625 MPa at 25°C to an average of 190 MPa at 1000°C, or 11 MPa/25°C. Unconfined, the reduction is non-linear from 350 MPa at 25°C to 35 MPa at 1000°C. The strength reduction for the basalt is also nearly linear to about 900°C; gradients are 8 MPa/25°C at 50-MPa confining pressure and 3 MPa/25°C unconfined. Our data are bracketed by those of Lindholm et al.[10] on Dresser Basalt (a little stronger) and Murrell and Chakravarty[1] on dolerite (a little weaker). Thus at 1000°C, the unconfined strengths of all three rocks are less than 100 MPa; only the granodiorite at 50 MPa-confining pressure remains fairly strong (~200 MPa).

(3) The strengths of the rocks vanish when even partial melting occurs. This takes place at a nominal temperature of about 1030°C at the hotter end of a basalt specimen. A few unconfined tests were done on andesite and granodiorite at about 1250°C (not listed). Nearly complete melting locally was achieved as would be expected as the liquidus temperatures of all phases range from 1100° to 1240°C.

We have determined the equivalent viscosity, $\eta = (\sigma_1-\sigma_3)/3\dot{\varepsilon}$, of the unconfined, partially melted rocks under a constant axial load due merely to the weight of the loading piston, about 0.1 MPa on the 2-cm specimens, by measuring the ensuing axial strain as a function of time (creep test). For andesite and granodiorite viscosities are of the order of 10^7 N • s/m^2, and for the lesser melted basalt about 10^9. These values agree well with those of Murase and McBirney[7] determined by a quite different technique, beam-bending.

(4) All three rocks are brittle throughout the temperature range explored until melting occurs. Shortenings at failure are less than 3 percent. Between 25° and 700°C the shortening at failure tends to be either constant or even to decrease.

(5) Most of the stress-shortening curves exhibit pronounced work-softening after the onset of macroscopic failure. This reflects displacement along faults that have not lost total resistance to differential stress.

(6) A few tests on the andesite and granodiorite were made at 10^{-7}/s, 25° and 400°C, unconfined and 50 MPa (Tables 1 and 2). Except for a 30 percent weakening of the andesite at room temperature and 50 MPa, the 1000-fold decrease in strain rate from 10^{-4}/s has negligible effects on strength or ductility.

(7) Two types of tests were made to investigate the cause(s) of the temperature-weakeing. All three rocks were first heated at 50-MPa confining pressure to temperatures between 750° and 1000°C, cooled to 25°C, and then deformed at confining pressure. The rocks are as strong after thermal cycling as before (Figs. 2, 3, 4), so that the thermal cracking caused by the relatively rapid heating and cooling (1.5°C/min or 10°C/min) is not the cause of strength reductions. Indeed, specimens of the andesite are an average of 25% stronger after thermal treatment (Figure 2), for reasons not yet understood. On the other hand, similar thermal treatment greatly reduces the strength of the unconfined rocks presumably because the effect of thermal cracking has not been suppressed by confining pressure.

In one inadvertant experiment, a specimen of andesite was heated to 980°C under 50-MPa confining pressure and then deformed (Fig. 1). During the shortening the internal furnace failed and the temperature fell to 880°C when the test was terminated at 6 percent strain, short of macroscopic failure. Instead of failing at 1 or 2 percent strain, as expected from previous experiments at constant temperature, the specimen work-hardened from 165 MPa at 930°C to 195 MPa at 900°C to >195 MPa at 880°C. The strengths at these temperatures fall on the curve established by constant-temperature experiments. These data need to be reproduced, but these preliminary results certainly suggest that temperature affects fracture strength, and does not merely degrade the strength of the rock through thermal cracking, at least under confining pressure.

Obsidian

Short term behavior. The strength and ductility of dry Newberry Rhyolite Obsidian has been determined at 0 and 50-MPa pressure, at temperatures to 800°C, and at a strain rate of 2×10^{-4}/s (Table 4). Ultimate strength decreases dramatically from 665 MPa at 600°C to 15 MPa at 800°C (Fig. 5); the brittle-ductile transition occurs between 600° and 700°C; and work-hardening ceases and steady-state flow obtains between 700° and 750°C.

Data at 50 MPa are not appreciably different (Table 4). Between 700° and 750°C the obsidian is somewhat stronger at 50 MPa than unconfined, but the opposite is true between 750° and 800°C. In short, the increment of 50 MPa in confining pressure has insignificant effects on short-time strength and ductility.

Time-dependent flow. Stress-relaxation tests[11,12] were made on 7 unconfined and 5 confined specimens (50 MPa) at temperatures between 700° and 800°C (Table 4). In these experiments, the loading pump is switched off at the end of the usual constant strain-rate path. The load supported by the specimen then decays with time as the stored elastic strains in the machine and specimen are converted into permanent strains within the specimen.

Assuming that the volume of hydraulic fluid in the loading ram remains constant during the relaxation, and that any anelastic relaxations of the machine are negligible, one can relate the permanent displacement, Δd_p, induced in the specimen to the force drop, ΔF, through the machine stiffness, k_m, and the specimen stiffness, k_s, as

$$\Delta d_p = -\left(\frac{1}{k_m} + \frac{1}{k_s}\right) \Delta F. \quad (1)$$

For specimens that are essentially inelastic (viscous) in behavior, the equation reduces to:

$$\Delta d_p = -\frac{1}{k_m} \Delta F. \quad (2)$$

Taking time derivatives, one can write

$$\dot{d}_p = -\frac{1}{k_m} \dot{F}. \quad (3)$$

Thus, by plotting curves of F against t and taking the gradient at specific points on the ensuing curve, one finds a data set relating F and $\dot{d}_p$, provided that the stiffnesses of the relevant parts of the machine are known. For these particular tests, the total machine stiffness, 1.23×10^8N/m is relevant. Strain rate, $\dot{\varepsilon}$, and differential stress $(\sigma_1-\sigma_3)$, are then calculated from the known length and cross-sectional area of the specimen at the start of the relaxation. Since the total induced strain during relaxation is very small (< 0.5%), it is not necessary to correct for changes in length or area. By this method we have obtained steady-state strength data at strain rates from 10^{-4} to 10^{-6}/s.

Equivalent viscosities. From data on $\dot{\varepsilon}$ and $(\sigma_1-\sigma_3)$ during relaxation, equivalent viscosities are calculated for a given temperature. Unconfined viscosities at 10^{-4} s^{-1} decrease from an average of 3.4×10^{11} at 700°C to about 3×10^{10} N · s/m^2 at 800°C. These values agree closely with those determined for this same obsidian at the same temperatures but with the beam-bending method by Murase and McBirney[7]. At 50-MPa confining pressure, the equivalent viscosities decrease with increasing temperature along a slightly steeper slope, but the effect of the pressure increment is insignificant. The specimens deformed at 50 MPa and 800°C were too weak for meaningful stress-relaxation testing (Table 4).

Plots of log $\dot{\varepsilon}$ against log $(\sigma_1-\sigma_3)$ show a systematic variation with temperature at both confining pressures (Fig. 6). The data fit a power law, $\dot{\varepsilon} \propto (\sigma_1-\sigma_3)^n$, with linear least-squares values for n ranging from about 2.0 at 700°C to about 1.6 at 800°C unconfined, and 1.3 to 1.5, confined.

Finally, a flow law of the type

$$\dot{\varepsilon} = A \exp(-Q/RT) (\sigma_1-\sigma_3)^n \quad (4)$$

is fit to the data between 700° and 800°C. The constant A is 2×10^{13} when σ is in MPa and $\dot{\varepsilon}$ is s^{-1}; the activation energy for viscous flow is Q = 380 kJ/mol; R is the gas constant; and $n \approx 1.5$. (By using n = 1.5, we ignore the very small effect of confining pressure.) Our value of Q agrees remarkably well with the 400 kJ/mol of Murase and McBirney[7]. We emphasize that this flow law has been determined only for temperatures between 700 and 800°C and $\dot{\varepsilon}$ from 10^{-4} to 10^{-6} s^{-1}, and that the parameter, n, varies with temperature and strain rate.

PETROFABRIC OBSERVATIONS

All specimens have been examined macroscopically, and thin- and polished-sections from over 50 specimens have been studied in detail to characterize the operative deformation mechanisms as functions of temperature and pressure. Quantitative data consist of the angle (θ) between the load axis (σ_1) and the macroscopic fault zone (Tables 1-4), microfracture abundance (e.g., Fig. 8), and chemical composition of glasses developed upon partial melting. These are accompanied by qualitative assessments of microfracture orientation and distribution, thermal alteration of minerals, gliding flow in mafic minerals, and development of glass in partially melted rocks.

Studies of deformation mechanisms are made to gain insight into temperature effects on strength and ductility. All the rocks deform primarily by brittle fracture until partial melting (crystalline rocks) or glass softening (obsidian) occurs.

Most specimens are shattered, i.e., they contain multiple faults (Tables 1-4). Only 50, 43, and 40 percent of the andesite, granodiorite and basalt specimens, respectively, contain a discrete fault from which a reliable measure of θ can be obtained. This angle ranges between 22° and 34° for the andesite, 24° and 35° for the granodiorite, and 28° and 42° for the basalt. In general, θ tends to increase with increasing temperature. There is a tendency for the fault zones to widen with increasing temperature and pressure.

By comparing the data from the few tests on the andesite at 25° and 400°C and 0 and 50 MPa done at strain rates of both 10^{-4} and 10^{-7}/s (Table 1), we note an unexpectedly large effect of time on the fracture angle, nearly 8°, not previously reported in the literature as far as we know.

Microscopically each fault zone (Fig. 7) consists of pervasive, precursive, extension microfractures (oriented within 20° of σ_1), and adjacent microscopic feather fractures[13,14]. Excellent examples are found of incipient faults along which en-echelon arrays of the precursive axial microfractures define the path of the eventual fault. Thermal fractures also occur; they are distinguishable by being relatively short, randomly oriented with respect to external coordinates, and located close to grain boundaries and/or larger fractures.

Detailed studies of microfracture abundances in the granodiorite and andesite have been made, and abundance is quantified as the average number of microfractures per mm intersected along linear traverses oriented perpendicular to the cylinder (load) axis: from 5 to 9 traverses with cumulative lengths of from 4.4 to 16.1 mm, spaced 2 to 5 mm apart for each specimen. Traverses across gouge either ignore it or are equated to discrete microfractures by arbitrarily assigning 100 microfractures for each millimeter of finely comminuted gouge. Both load-induced and thermoelastic fractures are counted. (A measure of the latter is afforded by study of specimens subjected only to thermal treatment.) Data for all three crystalline rocks are similar, and those shown for the granodiorite are representative (Fig. 8).

Clearly, the total number of both load-induced and thermal cracks increases with increasing temperature, about equally for all three rocks, and in the andesite about equally in the very-fine grained groundmass and in the phenocrysts. The increase in microfracture density of about 5 per mm from that in the starting material to that in specimens deformed at room temperature is essentially identical to that in the Westerly Granite under similar experimental conditions[15]. Subtracting the amount of thermal cracking from the total abundances of microfractures (Fig. 8), reveals that the degree of microfracturing caused by loading alone is about the same at all temperatures up to 1000°C, above which partial melting occurs and thermal cracking increases dramatically (not shown in the figure where up to 1000°C the increase is linear).

The work-softening exhibited by many of the specimens (Fig. 1) occurs during displacements along the macroscopic faults. Thin-section observations reveal that this softening is accompanied by local ductile flow in the groundmass of the andesite, the development of microscopic feather fractures and of gouge, and kinking of favorably oriented biotite and other types of gliding flow in mafic minerals immediately adjacent to the faults (Fig. 7). Some of these same mechanisms, along with thermal alteration of hornblende, biotite and pyroxene, probably also operate prior to macroscopic failure. However, in light of the strength and ductility trends, these mechanisms, if significantly influential at all, apparently contribute more to the weakening of the rocks than to the enhancement of their ductility, for virtually all of the permanent shortening is accountable to the macroscopic faulting in the brittle regime, even at 1000°C.

The partial melting in the crystalline rocks produces two types of glass. Under the microscope in transmitted light, one is brownish-amber, exhibits flow-banding, contains relatively few bubbles. Crystallites produced upon devitrification are common. The other glass is colorless and highly vesicular. Flow herein produces elongated vesicles. Electron-microprobe analyses by Drs. P. F. Hlava and E. J. Graeber of Sandia Laboratories confirm the petrologic evidence that the brownish-amber and clear glasses arise from melting of mafic minerals and feldspar, respectively.

BOREHOLE STABILITY

Ideally borehole stresses depend on the regional state of stress in the undisturbed rock, and this is not generally know a priori. Few measurements of the in-situ stress have been made in crystalline igneous rocks at depths of more than a few meters (Table 5). Using the hydraulic-fracturing technique, the staff of the Los Alamos Scientific Laboratory has determined the stress at a depth of 2926 m in the Precambrian crystalline basement of the Jemez Mountains in connection with its experiment on geothermal-energy extraction from dry hot rock. Taken as the weight per unit area of the superincumbent rock, the vertical stress, σ_v, is 72 MPa, and the minimum horizontal stress, σ_h, is 34 MPa[16]. Hydraulic-fracturing tests in granitic rocks in the United States[17] and basalt in Iceland[18] reveal that the horizontal stresses may be greater or less than the vertical stresses at depths in the range of 100 to 400 m. Strain-relief measurements in a South African dunite disclose an average horizontal stress at 350 m that greatly exceeds the overburden stress[19].

Since available data are too few for meaningful generalizations, we cannot predict the ratios of vertical to horizontal stresses elsewhere. For simplicity let us assume, therefore, that all horizontal stresses are equal and that σ_v/σ_h is 0.5, 1, or 2. Values falling much outside these extremes are unlikely, albeit possible.

At by far most locations where the complete in-situ stress tensor has been determined, σ_v is indeed equivalent to the weight per unit area of the overburden and it lies in a principal plane or close to it[20]. Let us assume that before the rock is drilled the state of stress is

$$\sigma_x = \sigma_y = \sigma_h$$
$$\sigma_z = \rho_r g z = \sigma_v \qquad (5)$$
$$\sigma_h = b\sigma_v,$$

where b = 0.5, 1, or 2; z (m) is depth below the free surface; ρ_r (kg/m^3) is the average bulk density of the overburden; g (m/s^2) is acceleration of gravity; and compressive stresses (MPa) are counted positive.

In cylindrical coordinates (Fig. 9) the vertical axial stress, σ_z', and the horizontal radial and tangential stresses, σ_r' and σ_θ', in the undisturbed rock are in general

$$\sigma_r' = \frac{\sigma_x + \sigma_y}{2} + \frac{\sigma_x - \sigma_y}{2}\cos 2\theta$$
$$\sigma_\theta' = \frac{\sigma_x + \sigma_y}{2} - \frac{\sigma_x - \sigma_y}{2}\cos 2\theta \qquad (6)$$
$$\sigma_z' = \rho_r g z,$$

where the angle θ is measured counterclockwise from the x direction, and $\sigma_x > \sigma_y$.

Now suppose that a vertical, perfectly cylindrical hole is drilled into the stressed mass of dry, statistically homogeneous and isotropic, ideally elastic rock. The original far-field stresses are perturbed in the vicinity of the hole where the new stresses can be computed from the Kirsch equations (see, for example, Ref. 21, p. 90-93).

$$\sigma_r = \frac{\sigma_x + \sigma_y}{2}\left(1 - \frac{a^2}{r^2}\right) + \frac{\sigma_x - \sigma_y}{2}\left(1 - \frac{4a^2}{r^2} + \frac{3a^4}{r^4}\right)\cos 2\theta$$
$$\sigma_\theta = \frac{\sigma_x + \sigma_y}{2}\left(1 + \frac{a^2}{r^2}\right) - \frac{\sigma_x - \sigma_y}{2}\left(1 + \frac{3a^4}{r^4}\right)\cos 2\theta, \qquad (7)$$

where a is the radius of the hole and σ_x and σ_y are the original far-field stresses. Since we are concerned with the stresses at the wall, let r = a. Then

$$\sigma_r = \tau_{r\theta} = 0$$
$$\sigma_\theta = \sigma_x + \sigma_y - 2(\sigma_x - \sigma_y)\cos 2\theta. \qquad (8)$$

The stress changes in plane strain are

$$\Delta\sigma_r = \sigma_r - \sigma_r' = -\left(\frac{\sigma_x + \sigma_y}{2}\right) + \left(\frac{\sigma_x - \sigma_y}{2}\right)\cos 2\theta$$
$$\Delta\sigma_\theta = \sigma_\theta - \sigma_\theta' = \frac{\sigma_x + \sigma_y}{2} - \frac{3(\sigma_x - \sigma_y)}{2}\cos 2\theta \qquad (9)$$
$$\Delta\sigma_z = \nu(\Delta\sigma_r + \Delta\sigma_\theta) = -2\nu(\sigma_x - \sigma_y)\cos 2\theta,$$

where ν = Poisson's ratio, about 0.25 for rock.

Adding these stress changes to the intial stresses (equation 6), assuming that $\sigma_x = \sigma_y = \sigma_h$ (equation 5), and solving for the maximum values at cos 2θ = 1 gives

$$\sigma_r = 0$$
$$\sigma_\theta = 2\sigma_h \qquad (10)$$
$$\sigma_z = \rho_r g z.$$

Since $\tau_{r\theta} = 0$, these are principal stresses.

For an average bulk density, $\rho_r = 2.7 \times 10^3$ kg/m^3, the vertical stress, σ_z, increases at the rate of 27 MPa/km.

Although well completions at near-magmatic temperature may require work in an open hole, let us suppose that a hydrostatic borehole pressure, p_b, can be maintained by a drilling fluid which cannot penetrate the surrounding impermeable rock. Then the stresses are

$$\sigma_r = p_b$$
$$\sigma_\theta = 2\sigma_h - p_b \qquad (11)$$
$$\sigma_z = \rho_r g z$$

Conventional, heavy, oil-well drilling muds can be formulated for a density as high as 2×10^3 kg/m^3, but they are not stable at the high temperatures of concern, so we suppose that the hole is filled with water with a density close to 1×10^3 kg/m^3 at 25°C. (The density is really less at high temperatures.) The borehole pressure, p_b, then increases at a rate of 10 MPa/km.

All crustal rocks have finite porosity, owing to intergranular voids and intragranular microcracks, and commonly to unsealed macrofractures as well. Let us suppose that these spaces are saturated with ground water under a hydrostatic pore-pressure, p_p, which increases at the rate of 10 MPa/km. To find the effective stresses, $\bar{\sigma}$, in the solid rock around the open borehole, we subtract p_p from all the normal stresses in equations 10 and 11. The vertical

stress, $\bar{\sigma}_z = (\rho_r - \rho_w)\, gz$, increases at a rate of about 17 MPa/km.

Should the wallrock be permeable, the pore pressure in the vicinity of an open hole would bleed off, and the stresses would approach those given by equation 10. Around the water-filled well the pore pressure and borehole pressures would equalize, and the stresses would approach those given by equation 11.

The principal stresses ($\sigma_1 > \sigma_2 > \sigma_3$) given by equations 10 and 11 together with differential stresses, σ_1-σ_3, and mean stresses, $\sigma_m = (\sigma_1 + \sigma_2 + \sigma_3)/3$, are given in Table 6 for the different ratios, σ_h/σ_v. Note that for a water-filled hole in water-saturated rock, the tangential stress can become tensile when the far-field horizontal stress is low relative to the overburden stress. This state of stress would favor unintentional hydraulic fracturing and lost circulation of the drilling fluid.

Our estimates of the borehole stresses should be regarded as minimal because the stresses are higher where $\sigma_x \neq \sigma_y$, as is commonly observed in nature, and because the walls of a real drillhole are not smooth, so that stress concentrations may be much higher than we have assumed ideally.

Recall that in the triaxial compression test the principal stresses are $\sigma_1 > \sigma_2 = \sigma_3 = P_c$, whereas in the wall of the borehole, $\sigma_1 > \sigma_2 > \sigma_3$. In order to use the laboratory data to predict failure of the borehole, we assume that ultimate compressive strength, σ_1-σ_3, at failure, is a function only of mean stress, $\sigma_m = (\sigma_1 + \sigma_2 + \sigma_3)/3$, and temperature. We realize that this strength is not independent of the relative magnitude of the intermediate principal stress, σ_2, and since we have measured it at only two different confining pressures (p_c = 0, 50 MPa), we must assume that it is linearly proportional to mean pressure. However, the effect of σ_2 is second-order[22], and the relation between strength and mean pressure is very nearly linear for many rocks in the brittle state[23,24]. Given all the other uncertainties of the predictions, we regard this failure criterion as good an approximation as any proposed[22].

Figure 10 shows an example of one way to associate strength data with borehole failure. Using the quantities listed in Table 6 for dry rock (p_p = 0) and the ratio, σ_h/σ_v = 1, we plot differential stress, σ_1-σ_3, as a function of mean pressure, σ_m, at the borehole wall for an open hole (p_b = 0) and a water-filled hole (p_b = 10 MPa/km) in impermeable rock. Choosing the proper stress gradients, σ_1-σ_3 = 54 and 34 MPa/km, respectively, we relate the stresses to depth below the surface. At any given depth, the borehole pressure reduces the differential stress and so tends to stabilize the hole.

On this diagram of the borehole stresses as functions of depth, we superimpose the plots of ultimate compressive strength versus mean pressure, using the data of Table 1 and Figure 2 for dry andesite at temperatures of 25°, 400°, 700°, and 900°C and confining pressures of 0 and 50 MPa. At a given mean pressure, say 50 MPa, the strengths exceed the borehole differential-stress, so that even the open hole is stable at all temperatures. The intersections of the two sets of curves mark the boundaries between the fields of stability, containing all points to the left of the loci of borehole stresses, and of instability, containing all points on the right-hand side. Since the strength curves are subparallel to each other and to the borehole-stress curves, these boundaries are not sharp. Nevertheless, they can be related approximately to depth, about 6, 4, 3, and 2 km at 25, 400, 700, and 900°C, respectively, for the open hole. The water-filled hole is stable at all temperatures to a depth of at least 10 km.

Table 7 gives the maximum depths for borehole stability, determined by the same procedure for all conditions treated in Table 6 and for both andesite and granodiorite. It appears that boreholes in these rocks would be stable even at 900°C unless the in-situ horizontal stresses are very high. The data on basalt are similar. The obsidian is even stronger than the crystalline rocks up to about 600°C, above which, however, it is much weaker, its strength approaching zero at 800°C.

Our predictions are likely to be optimistic. Recall that the borehole stresses would be higher than supposed if the far-field horizontal stresses were not equal and if the stress concentrations in a real hole were greater than those idealized for the calculations. Furthermore, we have not yet fully accounted for the effects of pore water and time.

We have emphasized the testing of room-dry rocks at a strain rate of 10^{-4}/s because data can be collected quickly and easily. The results are conservative in the sense that the measured strength is the highest and ductility is the lowest that can be expected. In other words, if a borehole in dry rock is potentially unstable under short-time loading, then it will surely fail under long-term loading or where the rock has been water-weakened.

The influence of pore water is twofold. The purely mechanical effect is to reduce the effective borehole stresses (Table 6), according to Terzaghi[25,26], and to extend somewhat the maximum depth of the stable field (Table 7). On the other hand, chemical effects--water weakening or stress corrosion--tend to lower ultimate compressive strength. The higher is the temperature, the more significant is this phenomenon likely to be[27].

Our own limited data and the previous work of others, as reviewed by Carter[3], show that lowering the strain rate or increasing the duration of loading in a creep test decrease strength even at low temperature. The higher is the temperature, the stronger is the time dependence, especially with approach to the melting point. We shall be investigating time effects in the immediate future.

CONCLUSIONS

The major conclusions to be drawn from the experimental and petrofabric results now available are as follows.

(1) The failure strengths of the crystalline rocks decrease gradually with increasing temperature to about 900°C, and then more rapidly as partial melting is approached between 1000° and 1100°C. The obsidian is even stronger than are the crystalline rocks up to 600°C, above which, however, the glass softens and strength vanishes at 800°C.

(2) The crystalline rocks are essentially brittle throughout the temperature range explored until partial melting occurs. They deform primarily by fracture, with some ductile flow in the groundmass where it is present, some gliding flow (kinking) in the biotite, and thermal alteration of the mafic minerals contributing to the strength reduction by an unknown, but probably minor amount. Shortenings at failure are less than 3 percent. Virtually all the permanent shortening is ascribable to macroscopic faulting.

(3) Several facts strongly suggest that the temperature-weakening of the crystalline rocks is due to intrinsic effects of temperature on the process leading to macroscopic shear fracturing (or faulting), and not merely to degradation of strength by thermal cracking, at least when the rocks are subjected to confining pressure. (1) Brittle fracture accounts for virtually all the permanent strain. (2) The degree of microfracturing associated with the mechanical loading, as distinguished from the thermoelastic stressing, is about the same at all temperatures from 25° to 1000°C. (3) Specimens heated to 1000°C cooled, and then deformed at 25°C are at least as strong as those that have not been preheated.

On the other hand, similar thermal cycling greatly degrades the strengths of the unconfined rocks, presumably because the effect of the thermal cracks on subsequent failure is not suppressed by confining pressure; that is, heating significantly modifies the mechanical state of the material. Thus, data from unconfined tests alone cannot be used for valid predictions of rock properties under in situ conditions particularly for geological or geophysical applications. However, such tests may be useful to estimate strengths during drilling where unconfined conditions and rapid cooling may obtain.

Several workers have regarded fracturing as a thermally-activated process, and by fitting their data to an equation of the form of equation 4, they have derived an apparent activation energy[4]. Owing to the lack of data on time effects, we cannot do so. However, even if brittle fracturing is indeed rate-controlled, how could we, or the previous workers for that matter, associate the purely empirical, apparent activation energy with a specific process? Is it the initiation and/or propagation of intragranular microfracturing? Is it grain-boundary sliding? Is it the condensation of microfracturing in preferred zones and/or the precursory coalescence that appears to cause the instability manifest in the macroscopic fracturing, stress drop, and work-softening that characterize the ultimate failure of these rocks? We claim that a lot more research on fracture must be done before a meaningful constitutive "law" can be written for inelastic deformations in the brittle state.

(4) Because the deformations of the rocks are essentially cataclastic at all temperatures, we suppose that the borehole will fail in shear when the differential stress reaches the ultimate compressive strength. A hole as deep as 10 km in the dry rocks under short-time loading is not likely to fail even at 1000°C unless the in-situ horizontal stress is equal to or greater than the vertical stress and the hole is open (Table 7).

(5) Our predictions of borehole stability are optimistic because we have not yet accounted for the effects of duration of loading (creep) and water-weakening which should significantly lower the strengths of the rocks at the higher temperatures. Assessment of these effects is the next objective of our research. Predictions must remain qualitative until sophisticated numerical methods can be applied to the problem. This cannot be done until adequate constitutive relations are known over the entire range of significant variables--at least of confining pressures from 0 to 200 MPa, temperatures from 25° to 1000°C, and times of a few seconds to several years--let alone the chemical effects of interstitial fluids.

ACKNOWLEDGMENTS

Dr. E. J. Graeber and his associates at Sandia Laboratories collected the starting blocks of Mt. Hood Andesite, Newberry Rhyolite Obsidian, and Cuerbio Basalt, supplied the X-ray photos of the vesicular basalt, and made the microprobe analyses of the glasses produced upon partial melting of the granodiorite. Mr. J. N. Magouirk and Dr. J. M. Logan helped in the design and construction of the high temperature apparatus. This work was supported by the Sandia Laboratories, Contract No. 82-9794, as part of their research program on energy extraction from magma.

REFERENCES

1. Murrell, S. A. F. and Chakravarty, S.: "Some New Rheological Experiments on Igneous Rocks at Temperatures up to 1120°C", Geophys. J. R. Astr. Soc., v. 34, p. 211-250 (1973).

2. Handin, J.: "Strength and Ductility", Section 11 In: Handbook of Physical Constants, Rev. Ed., Geol. Soc. America Mem. 97 (1966).

3. Carter, N. L.: "Steady State Flow of Rocks", Rev. Geophys. and Space Phys., v. 14, p. 301-357 (1976).

4. Carter, N. L. and Kirby, S. H.: "Transient Creep and Semibrittle Behavior of Crystalline Rocks", Pure and Applied Geophys., v. 116, p. 806-839 (1978).

5. Heard, H. C.: "Effect of Large Changes in Strain Rate in the Experimental Deformation of Yule Marble", J. Geol., v. 71, p. 162-195 (1963).

6. Goetze, C.: "High Temperature Rheology of Westerly Granite", J. Geophys. Res., v. 76, p. 1223-1230 (1971).

7. Murase, T. and McBirney, A. F.: "Properties of Some Common Igneous Rocks and Their Melts at High Temperatures", Geol. Soc. Am. Bull., v. 84, p. 3563-3592 (1973).

8. Krech, W. W., Henderson, F. A., and Hjelmstad, K. E.: "A Standard Rock Suite for Rapid Excavation Research", Bureau Mines, R.I. 7865, 29 p. (1974).

9. Friedman, M. and Bur, T. R.: "Investigation of the Relations Among Residual Strain, Fabric, Fracture, and Ultrasonic Attenuation and Velocity in Rocks", Int. J. Rock Mech. Min. Sci., v. 11, p. 221-234 (1974).

10. Lindholm, U. S., Yeakley, L. M., and Nagy, A.: "The Dynamic Strength and Fracture Properties of Dresser Basalt", Int. J. Rock Mech. Min. Sci., v. 11, p. 181-191 (1974).

11. Lee, D. and Hart, E. W.: "Stress Relaxation and Mechanical Behavior of Metals", Metall. Trans., v. 2, p. 1245-1248 (1971).

12. Rutter, E. H., Atkinson, B. K., and Mainprice, D. H.: "On the Use of the Stress Relaxation Testing Method in Studies of the Mechanical Behavior of Geological Materials", Geophys. J. R. Astro. Soc., v. 55(1), p. 155-170 (1968).

13. Friedman, M.: "Fracture in Rock", Rev. Geophys. and Space Phys., v. 13, p. 352-358 (1975).

14. Conrad, R. E., II and Friedman, M.: "Microscopic Feather Fractures in the Faulting Process", Tectonophysics, v. 33, p. 187-193 (1976).

15. Tapponnier, P. and Brace, W. F.: "Development of Stress-Induced Microcracks in Westerly Granite", Int. J. Rock Mech. Min. Sci., v. 12, p. 103-112 (1976).

16. Brown, D. W.: Personal Communication (1976).

17. Haimson, B. C.: "The Hydrofracturing Stress-Measuring Technique: Methods and Recent Field Results in the United States", Proc. Int. Symp. on Investigation of Stress in Rock, Inst. Engr., Sydney, Australia, p. 23-30 (1976).

18. Haimson, B. C. and Voight, B.: "Crustal Stress in Iceland", Pure and Appl. Geophys., v. 115, p. 1-38 (1977).

19. Gay, N. C.: "In-Situ Stress Measurements in Southern Africa", Tectonophysics, v. 29, p. 447-459 (1975).

20. Haimson, B. C.: "The Hydrofracturing Stress Measuring Method and Recent Field Results", Int. J. Rock Mech. Min. Sci., v. 15, p. 167-178 (1978).

21. Timoshenko, S. P. and Goodier, J. N.: "Theory of Elasticity", New York, McGraw-Hill (1970).

22. Handin, J., Heard, H. C., and Magouirk, J. N.: "The Effect of the Intermediate Principal Stress on the Failure of Limestone, Dolomite, and Glass at Different Temperatures and Strain Rates", J. Geophys. Res., v. 72, p. 611-640 (1967).

23. Handin, J. and Hager, R. V., Jr.: "Experimental Deformation of Sedimentary Rocks Under Confining Pressure: Tests at Room Temperature on Dry Samples", Am. Assoc. Petroleum Geologists Bull., v. 41, p. 1-50 (1957).

24. Borg, Iris and Handin, John: "Experimental Deformation of Crystalline Rocks", Tectonophysics, v. 3, p. 249-368 (1966).

25. Handin, J., Hager, R. V., Jr., Friedman, M., and Feather, J. N.: "Experimental Deformation of Sedimentary Rocks Under Confining Pressure: Pore Pressure Tests", Am. Assoc. Petroleum Geologists, v. 47, p. 717-755 (1963).

26. Brace, W. F. and Martin, R. J., III: A Test of the Law of Effective Stress for Crystalline Rocks of Low Porosity", Int. J. Rock Mech. Min. Sci., v. 5, p. 415-426 (1968).

27. Griggs, D. T.: "Hydrolytic Weakening of Quartz and Other Silicates", Geophys. J., v. 14, p. 19-31 (1967).

Table 1
Experimental data for mount hood andesite

SPECIMEN NO.	CONFINING PRESSURE (MPa)	TEMP. (°C)	MEAN STRESS (MPa)	ULTIMATE STRENGTH (MPa)	SHORTENING AT FAILURE (%)	COMMENTS[a] & FAULT ANGLE (θ°)
20	0	25	50	150	1.1	S
21	0	25	30	100	1.1	S
481[b]	0	25	35	110	0.8	S
482[b]	0	25	30	90	0.8	S
483[b]	0	25	40	115	1.3	23
493	0	400	50	145	1.3	S
496	0	400	35	110	1.2	S
499	0	400	35	105	1.2	23
503[b]	0	400	35	110	1.0	S
507[b]	0	400	45	135	1.1	30
36	0	700	40	115	1.0	25, S
37	0	700	35	100	0.9	S
8	50	25	155	320	2.3	27
225	50	25	135	250	3.2	S
27[b]	50	25	125	220	6.8	34
28[b]	50	25	125	220	6.9	32
9	50	400	125	230	2.7	32
16	50	400	150	305	1.8	32
31	50	700	130	235	0.9	I
34	50	700	130	235	1.6	I
84	0	1000	30	85	1.5	S
85	0	1000	25	75	1.5	S
97	50	1000	85	110	1.4	S
123[c]	50	930	105	165	1.6	
123[c]	50	900	115	195	3.5	
123[c]	50	880	115	195	5.4	
125[d]	50	25	180	390	2.1	32
128	50	25	140	275	2.0	32
221[e]	0	25	30	90	1.7	S
223[f]	0	25	40	120	1.5	S
226[g]	50	25	155	315	2.5	29

a. S = shattered (2 or more fractures or faults), I = incipient fault.

b. Strain rate is $10^{-7}s^{-1}$.

c. Specimen work-hardened during temperature decrease.

d. Specimen 125 was heated to 930°C at 10°C/min, cooled, and then deformed at 25°C and 50 MPa.

e. Unconfined specimen heated to 905°C at 1.5°C/min, cooled, and then deformed at 25°C.

f. Unconfined specimen heated to 1000°C at 1.5°C/min, cooled, and then deformed at 25°C.

g. Unconfined specimen heated to 1000°C at 1.5°C/min, cooled and then deformed at 25°C and 50 MPa.

Table 2
Experimental data for charcoal granodrite

SPECIMEN NO.	CONFINING PRESSURE (MPa)	TEMP (°C)	MEAN STRESS (MPa)	ULTIMATE STRENGTH (MPa)	SHORTENING AT FAILURE (%)	COMMENTS,[a] FAULT ANGLE (θ°)
22	0	25	120	360	0.8	S
24	0	25	115	340	0.6	S
38	0	400	40	115	1.0	S
44	0	400	40	115	0.8	S
511	0	400	60	175	1.3	S
512	0	400	60	175	1.1	18, S
513[b]	0	400	55	165	1.1	S
514[b]	0	400	55	160	1.1	S
564	50	25	270	665	2.1	29
T1	50	25	255	620	1.7	S
M3	50	25	260	630	1.8	35
T2	50	400	220	510	1.4	27
18	50	400	220	520	1.5	S
233	50	400	245	580	1.4	S
236	50	400	235	560	1.4	27
45	50	400	230	535	1.5	S
46	0	700	15	45	1.2	S
47	0	700	25	70	1.2	S
231	50	700	205	465	2.0	27, S
232	50	700	180	390	1.8	29, S
51	0	>1050	0	0	27.0	PM
86	0	1000	15	40	1.7	30, S
87	0	1000	10	30	1.9	30, S
118	50	1000	85	100	1.7	S
119	50	930	135	255	1.9	S
132	50	1000	140	275	1.8	36
133[c]	50	25	260	635	1.5	30
216[d]	0	25	20	55	1.8	S
217[e]	0	25	20	60	2.2	S
218[e]	0	25	20	60	1.8	S
227[g]	50	25	235	560	2.5	27

a. S = shattered (2 or more fractures [or faults]). PM = partial melting.
b. Strain rate is 10^{-7} sec^{-1}.
c. Confined specimen heated at 10°C/min to 1000°C and then deformed at 25°C and 50 MPa confining pressure.
d. Unconfined specimen heated to 1000°C at 10°C/min and then deformed at 25°C, unconfined.
e. Unconfined specimens heated to 900°C at 1.5°C/min and then deformed at 25°C, unconfined.
g. Unconfined specimen heated to 1000°C at 1.5°C/min, cooled and then deformed at 25°C and 50 MPa.

Table 3
Experimental data for cuerbio basalt

SPECIMEN NO.	CONFINING PRESSURE (MPa)	TEMP. (°C)	MEAN STRESS (MPa)	ULTIMATE STRENGTH (MPa)	SHORTENING AT FAILURE (%)	COMMENTS[a] & FAULT ANGLE (θ°)
201	0	25	100	300	0.8	S
204	0	25	100	305	0.8	S
196	0	575	70	210	0.6	S
208	0	900	70	205	1.2	S
212	0	1030	0	5	0.2	PM
202	50	25	185	400	1.6	S
203	50	25	230	540	1.2	28
209[b]	50	25	215	500	1.2	28
193	50	600	165	345	0.8	S
194	50	600	150	300	0.8	S
197	50	700	150	300	0.9	28
199	50	925	120	205	0.3	40, S
210	50	940	100	145	1.2	28
198	50	965	70	65	1.3	42
205	50	1000	80	95	1.4	UF
220[c]	0	25	70	210	1.4	S
222[d]	0	25	75	220	1.8	S
224	50	25	235	550	1.3	32, S

a. S = shattered (2 or more fractures or faults), PM = partial melting; UF = uniform flow and multiple fractures.

b. Specimen heated to 750°C at 10°C/min, cooled, and deformed at 25°C and 50 MPa.

c. Unconfined specimen heated to 905°C at 1.5°C/min, cooled, and deformed at 25°C.

d. Unconfined specimen heated to 1000°C at 1.5°C/min, cooled, and deformed at 25°C.

Table 4
Experimental data for newberry rhyolite obsidian

SPECIMEN NO.	CONFINING PRESSURE (MPa)	TEMP (°C)	MEAN STRESS (MPa)	ULTIMATE STRENGTH (MPa)	SHORTENING AT FAILURE (F) AT YIELDING (Y) (%)	COMMENTS[a] (%)
144	0	600	222	666	3.5 (F)	S
145	0	700	47	141	1.0-2.0 (Y)	6.2
135	0	700	76	228	2.0-4.0 (Y)	7.2
149	0	750	9	27	0.7 (Y)	3.8
151	0	750	10	30	0.6 (Y)	4.6
153'''[b]	0	770	17	50	0.5-1.0 (Y)	4.2
153'	0	800	5	14	0.6 (Y)	3.1
153''	0	800	5	15	0.4 (Y)	2.9
134	50	400	323	>820	4.1 (F)	S
168	50	700	155	315	0.8 (Y)	9.7
170	50	700	165	344	0.8 (Y)	9.0
172'''[b]	50	735	100	148	0.5 (Y)	5.3
169	50	750	80	91	0.5 (Y)	8.3
172''	50	765	61	32	0.1 (Y)	2.6
172'	50	800	52	5	0.1 (Y)	2.0
171	50	800	52	7	0.1 (Y)	6.8

a. S = shattered (2 or more fractures or faults), values in percent are the shortenings to which each specimen was taken and then allowed to relax. Specimens 171 and 172' were too weak to permit measurement of relaxation data.

b. Specimens 153 and 172 were each loaded cyclically in order '. '', and ''' of compression, relaxation, and recompression.

Table 5
Some in-situ stress measurements in igneous rocks

PLACE	ROCK	DEPTH (M)	VERTICAL (OVERBURDEN)	STRESSES (MPa) MAXIMUM HORIZONTAL	MINIMUM HORIZONTAL	REF.
CALIFORNIA	GRANITE	300	8.2	9.5	5.4	17
S. CAROLINA	GRANITE	230	6.2	22.8	15.9	17
WISCONSIN	GRANITE	136	3.5	16.0	7.0	17
N. MEXICO	GRANITE	2926	71.7	?	34.1	16
ICELAND	BASALT	203	5.4	6.3	4.1	18
ICELAND	BASALT	375	10.0	7.0	6.4	18
S. AFRICA	DUNITE	350	11.5	15.5 (average)		19

Table 6
Borehole stresses (MPa/km)

	CONDITION	σ_h/σ_v	σ_1	σ_2	σ_3	$\sigma_1-\sigma_3$	σ_m
DRY ROCK	OPEN HOLE	2	$\sigma_\theta = 108$	$\sigma_z = 27$	$\sigma_r = 0$	108	45
		1	$\sigma_\theta = 54$	$\sigma_z = 27$	$\sigma_r = 0$	54	27
		0.5	$\sigma_\theta = 27$	$\sigma_z = 27$	$\sigma_r = 0$	27	18
	FILLED HOLE	2	$\sigma_\theta = 98$	$\sigma_z = 27$	$\sigma_r = 10$	88	45
		1	$\sigma_\theta = 44$	$\sigma_z = 27$	$\sigma_r = 10$	34	27
		0.5	$\sigma_z = 27$	$\sigma_\theta = 17$	$\sigma_r = 10$	17	18
SATURATED ROCK	OPEN HOLE	2	$\bar{\sigma}_\theta = 88$	$\bar{\sigma}_z = 17$	$\bar{\sigma}_r = 0$	88	35
		1	$\bar{\sigma}_\theta = 34$	$\bar{\sigma}_z = 17$	$\bar{\sigma}_r = 0$	34	17
		0.5	$\bar{\sigma}_z = 17$	$\bar{\sigma}_\theta = 7$	$\bar{\sigma}_r = 0$	17	8
	FILLED HOLE	2	$\bar{\sigma}_\theta = 78$	$\bar{\sigma}_z = 17$	$\bar{\sigma}_r = 10$	68	35
		1	$\bar{\sigma}_\theta = 24$	$\bar{\sigma}_z = 17$	$\bar{\sigma}_r = 10$	14	17
		0.5	$\bar{\sigma}_z = 17$	$\bar{\sigma}_r = 10$	$\bar{\sigma}_\theta = -3$	20	8

$\sigma_z = \sigma_v = \rho_r gz = 27$ MPa/km for $\rho_r = 2.7 \times 10^3$ kg/m^3.

$p_b = p_p = \rho_w gz = 10$ MPa/km for $\rho_w = 10^3$ kg/m^3.

Table 7
Maximum depth (km) of a stable borehole

CONDITIONS			σ_h/σ_v	25°C	400°C	700°C	900°C
ANDESITE	DRY	OPEN HOLE	2.0	2	2	1	1
			1.0	6	4	3	2
			0.5	>10	>10	>10	>10
		FILLED HOLE	2.0	4	3	2	1
			1.0	>10	>10	>10	>10
			0.5	>10	>10	>10	>10
	SATURATED	OPEN HOLE	2.0	2	2	1	1
			1.0	9	7	5	4
			0.5	>10	>10	>10	>10
		FILLED HOLE	2.0	5	4	3	2
			1.0	>10	>10	>10	>10
			0.5	*	*	*	*
GRANODIORITE	DRY	OPEN HOLE	2.0	6	3	1	> 1
			1.0	>10	>10	>10	2
			0.5	>10	>10	>10	>10
		FILLED HOLE	2.0	>10	>10	6	1
			1.0	>10	>10	>10	>10
			0.5	>10	>10	>10	>10
	SATURATED	OPEN HOLE	2.0	6	3	> 1	1
			1.0	>10	>10	>10	> 2
			0.5	>10	>10	>10	>10
		FILLED HOLE	2.0	>10	>10	>10	2
			1.0	>10	>10	>10	>10
			0.5	*	*	*	*

*TANGENTIAL STRESS IS TENSILE.

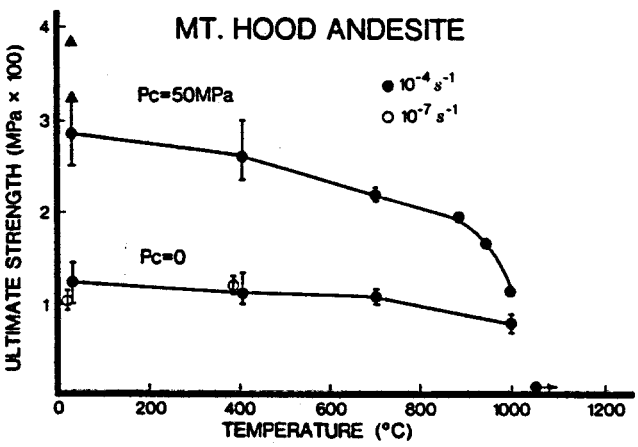

Fig. 2 - Ultimate strength versus temperature for Mt. Hood Andesite. Triangles (▲) represent specimens heated to 930-1000 C°, cooled, and deformed at 25 C°, 50 MPa. The unconfined strength at 25 C° is virtually the same whether or not a specimen has been preheated and cooled.

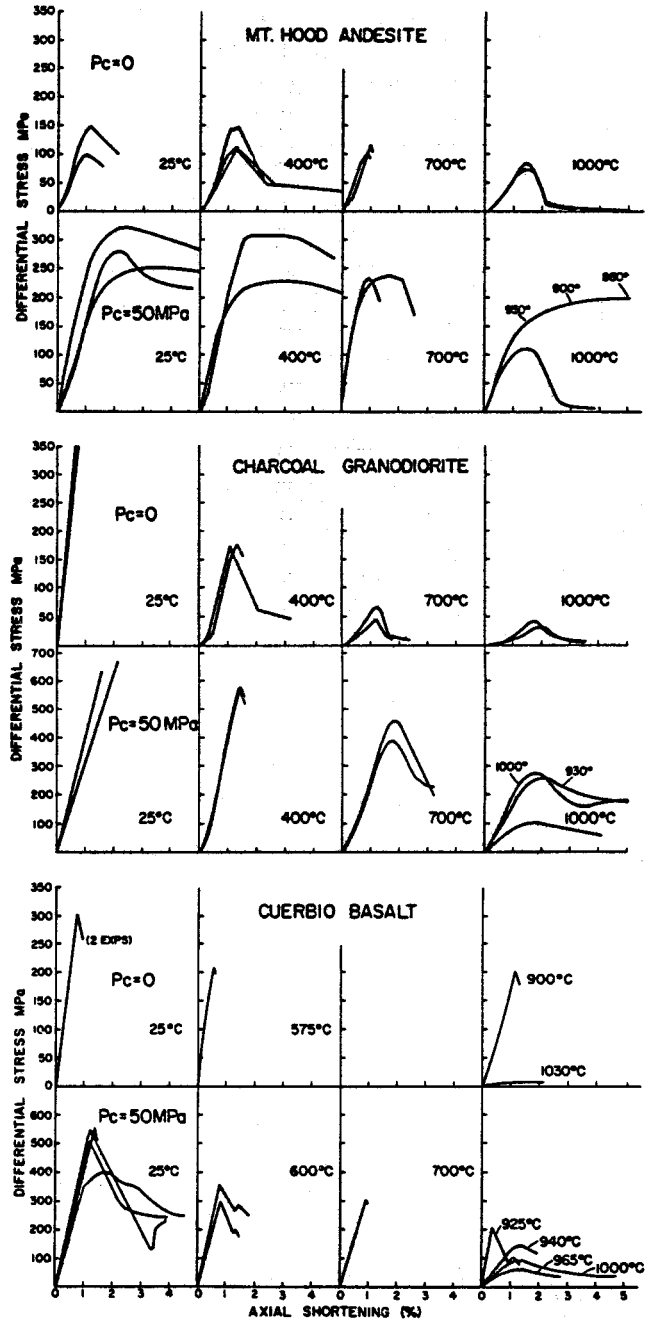

Fig. 1 - Stress-shortening curves for three crystalline rocks deformed at confining pressure (P_c) and temperatures shown.

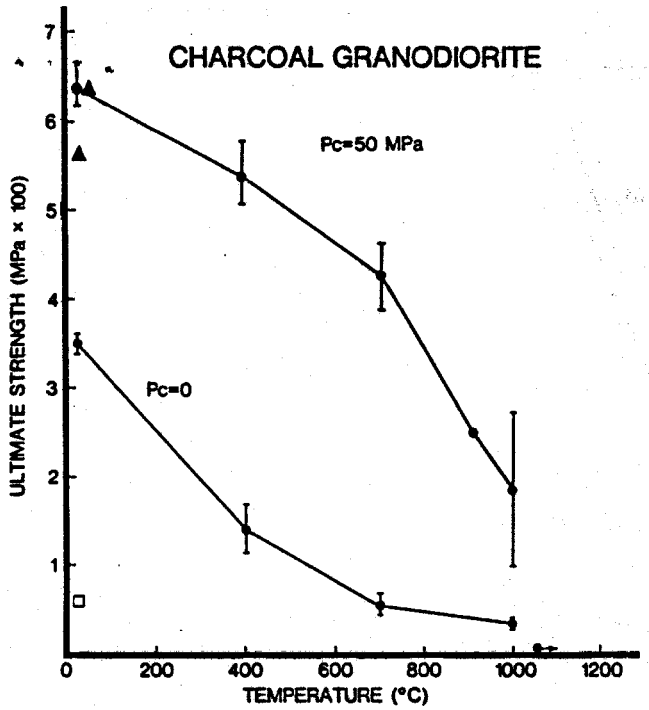

Fig. 3 - Ultimate strength versus temperature for charcoal granodiorite. Triangles (▲) represent specimens heated to 1000°C, cooled, and deformed at 25°C, 50 MPa. Open square (□) represents three unconfined specimens heated to 900-1000°C, cooled, and then deformed at 25°C.

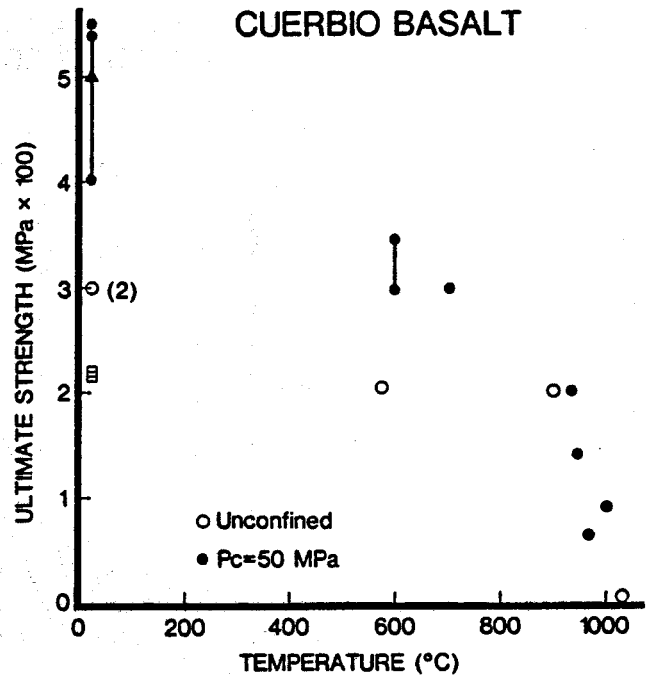

Fig. 4 - Ultimate strength versus temperature for cuerbio basalt. Triangle (▲) represents specimen heated to 750°C, cooled, and deformed at 25°C, 50 MPa. Open squares (□) represent unconfined specimens heated to 905-1000°C, cooled and then deformed at 25°C.

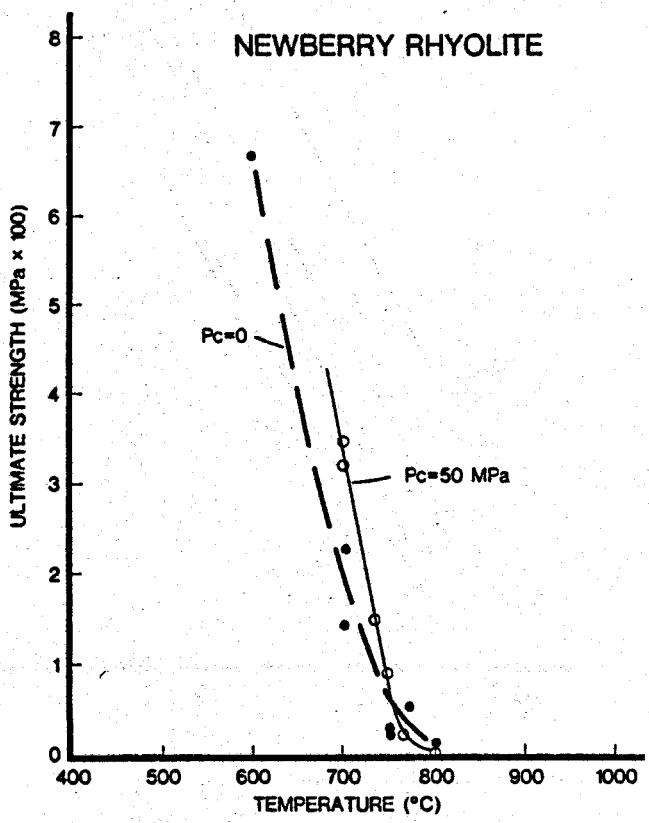

Fig. 5 - Ultimate strength versus temperature for Newberry rhyolite obsidian.

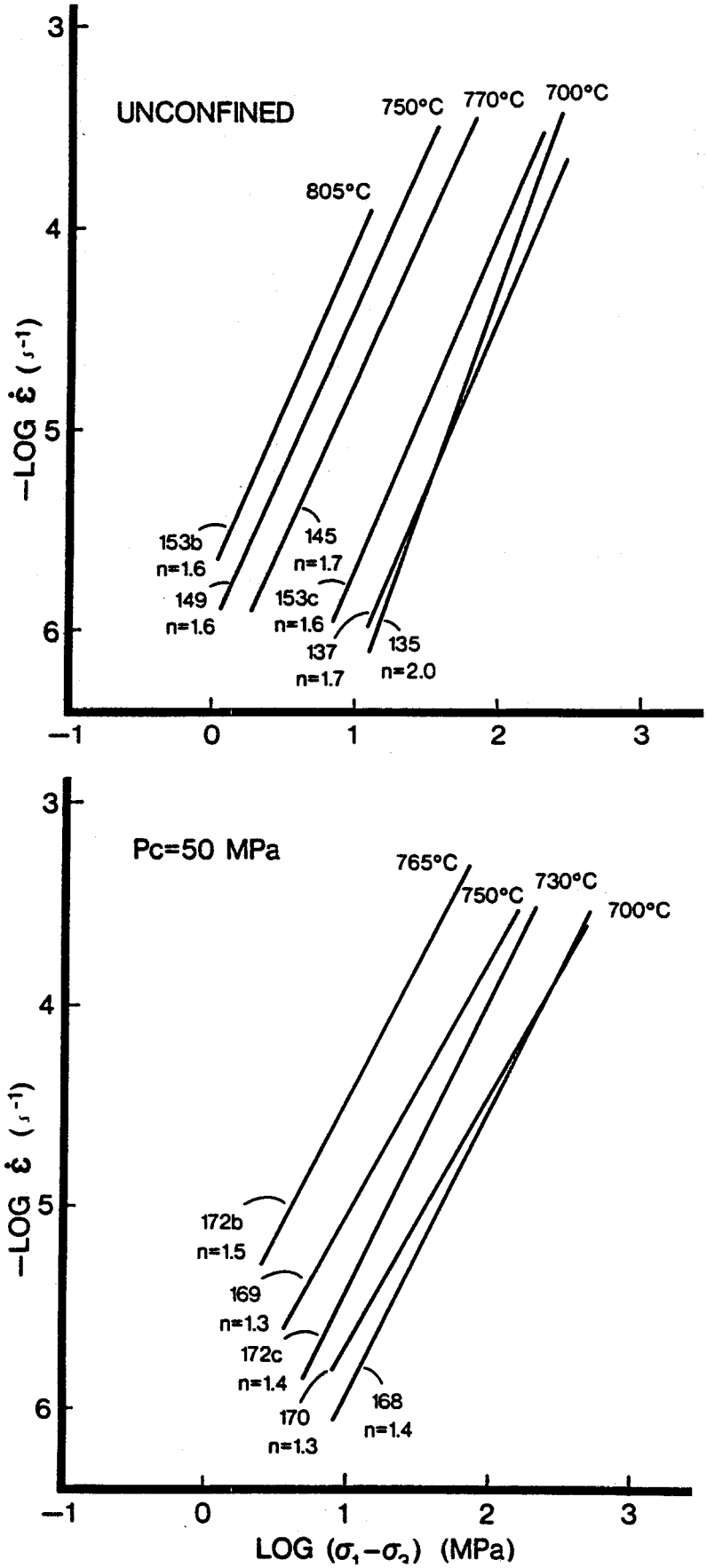

Fig. 6 - Log strain rate versus log steady-state flow stress for Newberry rhyolite obsidian at different temperatures and confining pressures (equation 4).

(a) Right-lateral fault zone in granodiorite specimen 132 (50 MPa) consists of gouge (G), Riedel shears (R_1), sheared opaque minerals, and microscopic feather fractures (thin arrow). Plane polarized light.

(b) Left-lateral shear zone in specimen 132 shows intense fracturing prior to development of fine-grain gouge. Partially crossed polarized light.

(c) Feldspar phenocryst in andesite (specimen 85) contains axial extension fractures. Crossed polarized light.

Fig. 7 - Photomicrographs of granodiorite and andesite deformed at 1000°C, showing that brittle fracture is the predominant mechanism of failure. The load axis (σ_1) is parallel to the long axis of each photo. Scale line is 0.5 mm for (a) and 0.2 mm for (b and c).

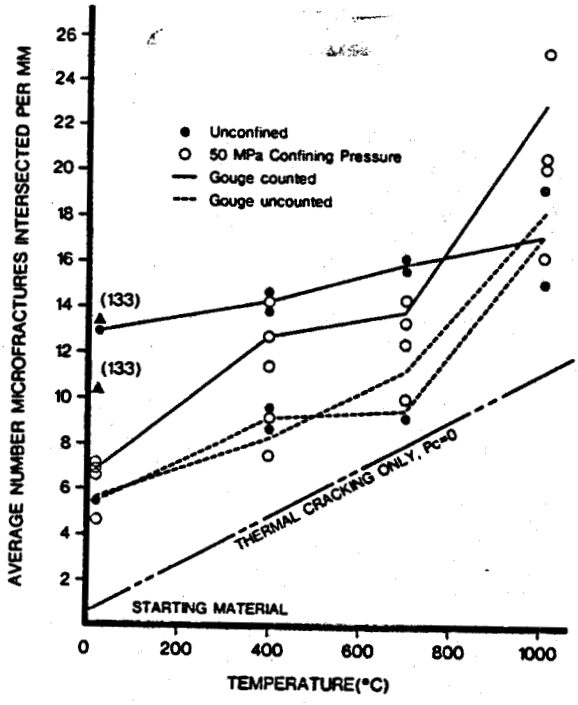

Fig. 8 - Microfracture abundance as functions of pressure and temperature in temperature deformed charcoal granodiorite. Specimen 133 (▲) was heated to 1000°C, cooled, deformed at 25°C, MPa; the higher result includes gouge, the lower does not.

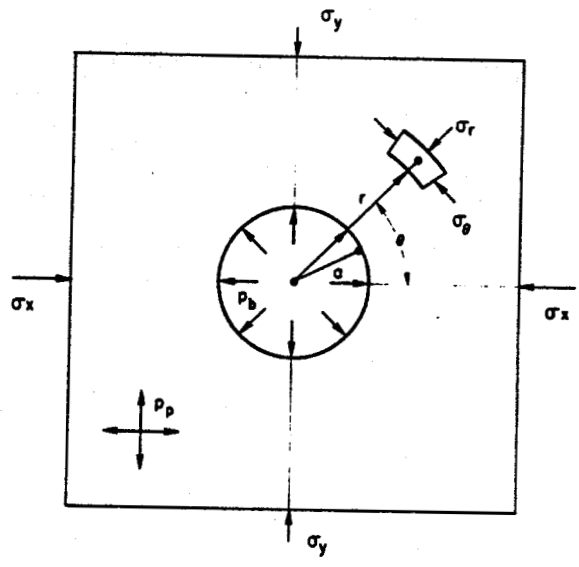

Fig. 9 - Radial and tangential stresses, σ_r and σ_θ, around a cylindrical hole of radius, a, in an elastic, isotropic plate. Far-field horizontal stresses are $\sigma_x > \sigma_y$; vertical stress is σ_z. Borehole fluid pressure is p_b, and pore pressure in a porous medium is p_p.

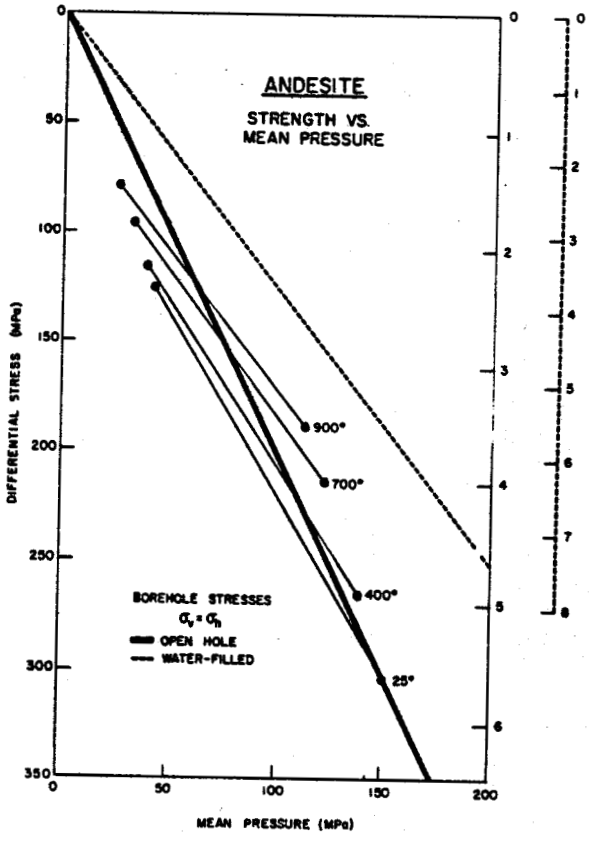

Fig. 10 - Differential stress versus mean pressure at wall of an open and water-filled borehole in impermeable rock (Table 6). Superposed are plots of ultimate compressive strength versus means pressure.

DISCLAIMER

This report was prepared as an account of work sponsored by an agency of the United States Government. Neither the United States Government nor any agency thereof, nor any of their employees, makes any warranty, express or implied, or assumes any legal liability or responsibility for the accuracy, completeness, or usefulness of any information, apparatus, product, or process disclosed, or represents that its use would not infringe privately owned rights. Reference herein to any specific commercial product, process, or service by trade name, trademark, manufacturer, or otherwise does not necessarily constitute or imply its endorsement, recommendation, or favoring by the United States Government or any agency thereof. The views and opinions of authors expressed herein do not necessarily state or reflect those of the United States Government or any agency thereof.